FUZZY SECOND ORDER SLIDING MODE CONTROL OF A DOUBLY-FED INDUCTION MACHINE SUPPLIED BY TWO MATRIX CONVERTERS

Zinelaabidine. BOUDJEMA **Rachid. TALEB**
Laboratoire Génie Electrique et Energies Renouvelables (LGEER), Electrical Engineering Department,
Hassiba Benbouali University, Chlef, Algeria.
boudjemaa1983@yahoo.fr r.taleb@univ-chlef.dz

Adil YAHDOU **Abdelkader BOUYEKNI**
Electrical Engineering Department, Hassiba Benbouali University, Chlef, Algeria.
yahdou10h@yahoo.fr a.bouyekni@univ-chlef.dz

Abstract: *Traditional vector control structures which include proportional-integral (PI) regulator for the speed DFIMs driven have some disadvantages such as parameter tuning complications, mediocre dynamic performances and reduced robustness. Thus, based on the analysis of the mathematical model of a DFIM supplied by two direct matrix converters, this paper addresses a non-linear control algorithm based on fuzzy logic and second order sliding mode. The conventional sliding mode control has large chattering on the electromagnetic torque developed by the DFIM. In order to solve this problem, the second order sliding mode technique with fuzzy logic functions is used. The simulation results show the effectiveness of the proposed method especially in chattering-free behavior, response to sudden load torque variations and robustness against machine parameters variations.*

Key words: *Doubly fed induction machine (DFIM); matrix converter; second order sliding mode; fuzzy logic.*

1. Introduction

The doubly fed induction machine (DFIM) is a very interesting solution for variables speed applications such as wind energy conversion systems and electric vehicles [1,2]. Therefore, it covers all power ranges. Obviously, the requested variable speed domain and the desired performances depend on the application types [3].

The DFIM has several different advantages compared to the usual squirrel-cage machine. The DFIM can be controlled from the stator or rotor by different possible combinations [4].

In [5], a study on a DFIM with constant stator frequency and vector control is described. DFIM stator is directly supplied by the grid, and a cyclo-converter feeds the rotor windings. The main drawback of this configuration is the speed operating range limited to 20%-25% of the nominal speed.

A novel high-power inverter drive system is exposed in [6,7]. Principles and experimental investigations are presented and discussed. The authors used a DFIM configuration that is supplied by pulse width modulation (PWM) inverters that are linked with current controllers. In this configuration, each side of the machine is fed by a dc-link ac/ac inverter. The stator and the rotor windings do not have the same voltage rating; a step-down transformer between the ac network and the three-phase rectifier of the rotor winding supply is added. This drive can be used in industrial applications, such as steel rolling mill or marine propulsion systems.

Currently the three phase matrix converters have received considerable attention because they may become a good alternative to voltage-source inverter Pulse Width-Modulation (PWM) topology. This is because the matrix converter provides bi-directional power flow, nearly sinusoidal input/output waveforms, and a controllable input power factor [8]. Furthermore, the matrix converter allows a compact design due to the lack of dc-link capacitors for energy storage. Consequently, in this work, a novel high-power bi-converter structure to supply a doubly fed induction machine (DFIM) is presented. Two matrix converter (MC) feed the stator and rotor windings. The outputs of the two MCs are combined electro-mechanically in the machine, and as a result, novel features can be obtained. For example, for high power drive applications, this configuration use two MCs dimensioned for a half of the DFIM power.

A lot of works have been presented with diverse control diagrams of DFIM. These control diagrams are usually based on vector control notion with conventional PI controllers.

Recently, the sliding mode control (SMC) method has been widely used for robust control of nonlinear

systems. Several papers have been published based on (SMC) of DFIG [9,10].

The SMC achieves robust control by adding a discontinuous control signal across the sliding surface, satisfying the sliding condition. Nevertheless, this type of control has an essential disadvantage, which is the chattering phenomenon caused by the discontinuous control action. To treat these difficulties, several modifications to the original sliding control law have been proposed, the most popular being the boundary layer approach [11, 12].

Fuzzy logic is a technology based on engineering experience and observations. In fuzzy logic, an exact mathematical model is not necessary because linguistic variables are used to define system behavior rapidly. One way to improve sliding mode controller performance is to combine it with fuzzy logic to form a fuzzy sliding mode controller (FSMC). The design of a sliding mode controller incorporating fuzzy control helps in achieving reduced chattering, simple rule base, and robustness against disturbances and nonlinearities.

The paper is structured as follows: the matrix converter modeling is discussed in Section 2. In Section 3, the doubly fed induction machine (DFIM) model and the vector control strategy are presented. Session 4 shows the synthesis of the different controllers applied on the speed control of the DFIM. The effectiveness of the proposed controller (FSOSMC) verified by simulation is presented in section 6. Finally, the main conclusions of the work are drawn.

2. The matrix converter model

The matrix converter performs the power conversion directly from AC to AC without any intermediate dc link. It is very simple in structure and has powerful controllability. The converter consists of a matrix of bi-directional switches linking two independent three-phase systems. Each output line is linked to each input line via a bi-directional switch.

Figure 1 shows the basic diagram of a matrix converter.

The switching function of a switch S_{mn} in figure 1 is given by :

$$S_{mn} = \begin{cases} 1 & S_{mn} \text{ closed} \\ 0 & S_{mn} \text{ open} \end{cases} \quad m \in \{A,B,C\}, n \in \{a,b,c\} \qquad (1)$$

The mathematical expression that represents the operation of the matrix converter in figure 1 can be

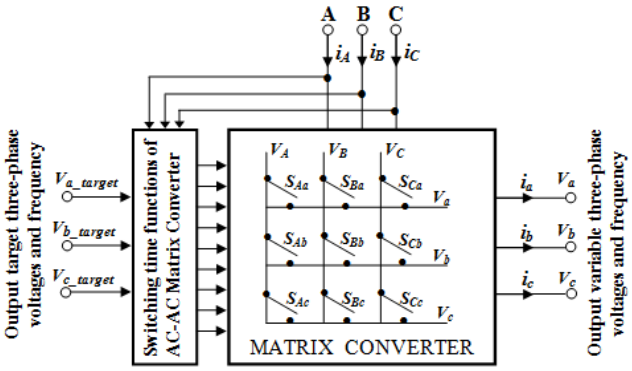

Fig. 1. Schematic representation of the matrix converter.

written as [12,13]:

$$\begin{bmatrix} V_a \\ V_b \\ V_c \end{bmatrix} = \begin{bmatrix} S_{Aa} & S_{Ab} & S_{Ac} \\ S_{Ba} & S_{Bb} & S_{Bc} \\ S_{Ca} & S_{Cb} & S_{Cc} \end{bmatrix} \cdot \begin{bmatrix} V_A \\ V_B \\ V_C \end{bmatrix} \qquad (2)$$

$$\begin{bmatrix} i_A \\ i_B \\ i_C \end{bmatrix} = \begin{bmatrix} S_{Aa} & S_{Ba} & S_{Ca} \\ S_{Ab} & S_{Bb} & S_{Cb} \\ S_{Ac} & S_{Bc} & S_{Cc} \end{bmatrix}^T \cdot \begin{bmatrix} i_a \\ i_b \\ i_c \end{bmatrix} \qquad (3)$$

To determine the behavior of the matrix converter at output frequencies well below the switching frequency, a modulation duty cycle can be defined for each switch.

The input/output relationships of voltages and currents are related to the states of the nine switches and can be expressed as follows :

$$\begin{bmatrix} V_a \\ V_b \\ V_c \end{bmatrix} = \begin{bmatrix} k_{Aa} & k_{Ab} & k_{Ac} \\ k_{Ba} & k_{Bb} & k_{Bc} \\ k_{Ca} & k_{Cb} & k_{Cc} \end{bmatrix} \cdot \begin{bmatrix} V_A \\ V_B \\ V_C \end{bmatrix} \qquad (4)$$

$$\begin{bmatrix} i_A \\ i_B \\ i_C \end{bmatrix} = \begin{bmatrix} k_{Aa} & k_{Ba} & k_{Ca} \\ k_{Ab} & k_{Bb} & k_{Cb} \\ k_{Ac} & k_{Bc} & k_{Cc} \end{bmatrix}^T \cdot \begin{bmatrix} i_a \\ i_b \\ i_c \end{bmatrix} \qquad (5)$$

$$\text{With} : 0 \le k_{mn} \le 1, \quad m = A, B, C, \quad n = a, b, c \qquad (6)$$

The variables k_{mn} are the duty cycles of the nine switches S_{mn} and can be represented by the duty-cycle matrix k. In order to prevent a short circuit on the input side and ensure uninterrupted load current flow, these duty cycles must satisfy the three following constraint conditions :

$$k_{Aa} + k_{Ab} + k_{Ac} = 1 \qquad (7)$$
$$k_{Ba} + k_{Bb} + k_{Bc} = 1 \qquad (8)$$
$$k_{Ca} + k_{Cb} + k_{Cc} = 1 \qquad (9)$$

The high-frequency synthesis technique introduced by Venturini (1980) and Alesina and Venturini (1988), allows a control of the S_{mn} switches so that the low frequency parts of the synthesized output voltages (V_a, V_b and V_c) and the input currents (i_A, i_B and i_C) are purely sinusoidal with the prescribed values of the output frequency, the input frequency, the displacement factor and the input amplitude.

The output voltage is given by :

$$\begin{bmatrix} V_a \\ V_b \\ V_c \end{bmatrix} = \begin{bmatrix} 1+2\delta\cos\alpha & 1+2\delta\cos(\alpha-\frac{2\pi}{3}) & 1+2\delta\cos(\alpha-\frac{4\pi}{3}) \\ 1+2\delta\cos(\alpha-\frac{4\pi}{3}) & 1+2\delta\cos\alpha & 1+2\delta\cos(\alpha-\frac{2\pi}{3}) \\ 1+2\delta\cos(\alpha-\frac{2\pi}{3}) & 1+2\delta\cos(\alpha-\frac{4\pi}{3}) & 1+2\delta\cos\alpha \end{bmatrix} \cdot \begin{bmatrix} V_A \\ V_B \\ V_C \end{bmatrix} \quad (10)$$

Where : $\begin{cases} \alpha = \omega_m + \theta \\ \omega_m = \omega_{output} - \omega_{input} \end{cases}$

The running matrix converter with Venturini algorithm generates at the output a three-phases sinusoidal voltages system having in that order pulsation ω_m, a phase angle θ and amplitude $\delta.V_s$ ($0 < \delta < 0.866$ with modulation of the neural) [14,15].

3. The DFIM model

Its dynamic model expressed in the synchronous reference frame is given by :

$$\begin{aligned} \bar{V}_S &= R_S\bar{I}_S + \frac{d\bar{\varphi}_S}{dt} + j\omega_S\bar{\varphi}_S \\ \bar{V}_R &= R_R\bar{I}_R + \frac{d\bar{\varphi}_R}{dt} + j\omega_R\bar{\varphi}_R \end{aligned} \quad (11)$$

$$\begin{aligned} \bar{\varphi}_S &= L_S\bar{I}_S + M_{SR}\bar{I}_R \\ \bar{\varphi}_R &= L_R\bar{I}_R + M_{SR}\bar{I}_S \end{aligned} \quad (12)$$

From (11) and (12), the state-all-current model is written as :

$$\begin{aligned} \frac{d\bar{I}_S}{dt} &= -\frac{R_S}{\sigma L_S}\bar{I}_S + \frac{M_{SR}R_R}{\sigma L_S L_R}\bar{I}_R + \frac{1}{\sigma L_S}\bar{V}_S - \frac{M_{SR}}{\sigma L_S L_R}\bar{V}_R \\ \frac{d\bar{I}_R}{dt} &= -\frac{R_R}{\sigma L_R}\bar{I}_R + \frac{M_{SR}R_S}{\sigma L_S L_R}\bar{I}_S + \frac{1}{\sigma L_R}\bar{V}_R - \frac{M_{SR}}{\sigma L_S L_R}\bar{V}_S \end{aligned} \quad (13)$$

This electrical model is completed by mechanical equation :

$$C_{em} - \frac{f\omega}{p} - C_r = \frac{J}{p}\frac{d\omega}{dt} \quad (14)$$

With :

$$\begin{cases} \omega = p\Omega \\ C_{em} = pM_{SR}.\mathrm{Im}(\bar{I}_S\bar{I}_S^{\,*}) \end{cases} \quad (15)$$

4. Control strategy of the DFIM

A. Rotor flux orientation

In this section, the DFIM model can be described by the following state equations whose axis *d* is aligned with the rotor flux vector (see figure 2) [16] :

$$\varphi_{Rq} = 0 \;\; ; \;\; \varphi_R = \varphi_{Rd} \quad (16)$$

So, using equation (12) we can write :

$$I_{Rq} = -\frac{M_{SR}}{L_R}.I_{Sq} \quad (17)$$

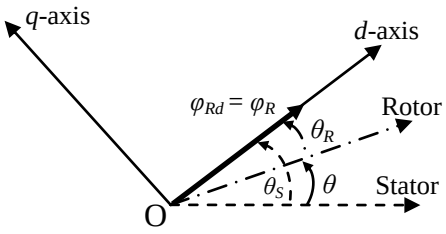

Fig. 2. Rotor field orientation on the *d*-axis.

Two methods can be used for motor magnetization [16] :

- Work with a unit power-factor in the stator or the rotor, which implies that one of the two currents, I_{Sd} or I_{Rd}, will be equal to zero,
- Divide the magnetizing current to equality between the two converters as follows :

$$I_{Sd} = I_{Rd} = \frac{I_d}{2}, \;\; \text{soit : } \varphi_{Rd} = (L_R + M_{SR})\frac{I_d}{2} \quad (18)$$

Choose $I_{Rd} = 0$ give the same expression to the stator and air-gap flux [16]. Moreover, the flux expression depends only on M_{SR} and the rotor power-factor will be equal the unit.

B. The current loops design

In order to obtain a decoupling between *d* and *q* axis, let us define new voltages as [16] :

$$\begin{cases} V_{tSq} = V_{Sq} - \frac{M_{SR}}{L_R}V_{Rq} \\ V_{tRq} = V_{Rq} - \frac{M_{SR}}{L_S}V_{Sq} \end{cases}, \begin{cases} V_{tSd} = V_{Sd} - \frac{M_{SR}}{L_R}V_{Rd} \\ V_{tRd} = V_{Rd} - \frac{M_{SR}}{L_S}V_{Sd} \end{cases} \quad (19)$$

Using equations (12), (16) and (19), we can write :

$$\begin{cases} V_{tSd} = R_S I_{Sd} + \sigma L_S \dfrac{dI_{Sd}}{dt} - R_R \dfrac{M_{SR}}{L_R} I_{Rd} - \varphi_{Sq}\omega_S + \dfrac{M_{SR}}{L_R}\varphi_{Rq}\omega_R \\ V_{tSq} = R_S I_{Sq} + \sigma L_S \dfrac{dI_{Sq}}{dt} - R_R \dfrac{M_{SR}}{L_R} I_{Rq} + \varphi_{Sd}\omega_S - \dfrac{M_{SR}}{L_R}\varphi_{Rd}\omega_R \\ V_{tRd} = R_R I_{Rd} + \sigma L_R \dfrac{dI_{Rd}}{dt} - R_S \dfrac{M_{SR}}{L_S} I_{Sd} - \varphi_{Rq}\omega_R + \dfrac{M_{SR}}{L_S}\varphi_{Sq}\omega_S \\ V_{tRq} = R_R I_{Rq} + \sigma L_R \dfrac{dI_{Rq}}{dt} - R_S \dfrac{M_{SR}}{L_S} I_{Sq} + \varphi_{Rd}\omega_R - \dfrac{M_{SR}}{L_S}\varphi_{Sd}\omega_S \end{cases} \quad (20)$$

Thus:

$$\begin{cases} V_{tSd} = V_{tSdc} + V_{tSdc1} = R_S I_{Sd} + \sigma L_S \dfrac{dI_{Sd}}{dt} + V_{tSdc1} \\ V_{tSq} = V_{tSqc} + V_{tSqc1} = R_S I_{Sq} + \sigma L_S \dfrac{dI_{Sq}}{dt} + V_{tSqc1} \\ V_{tRd} = V_{tRdc} + V_{tRdc1} = R_R I_{Rd} + \sigma L_R \dfrac{dI_{Rd}}{dt} + V_{tRdc1} \\ V_{tRq} = V_{tRqc} + V_{tRqc1} = R_R I_{Rq} + \sigma L_R \dfrac{dI_{Rq}}{dt} + V_{tRqc1} \end{cases} \quad (21)$$

This method gives the same transfer function between the currents and voltages of the same axis as shown by the following equation :

$$\begin{cases} \dfrac{I_{Sq}(s)}{V_{tSqc}(s)} = \dfrac{I_{Sd}(s)}{V_{tSd}(s)} = \dfrac{1}{R_S + \sigma L_S \,.\, s} \\ \dfrac{I_{Rq}(s)}{V_{trqc}(s)} = \dfrac{I_{Rd}(s)}{V_{tRd}(s)} = \dfrac{1}{R_R + \sigma L_R \,.\, s} \end{cases} \quad (22)$$

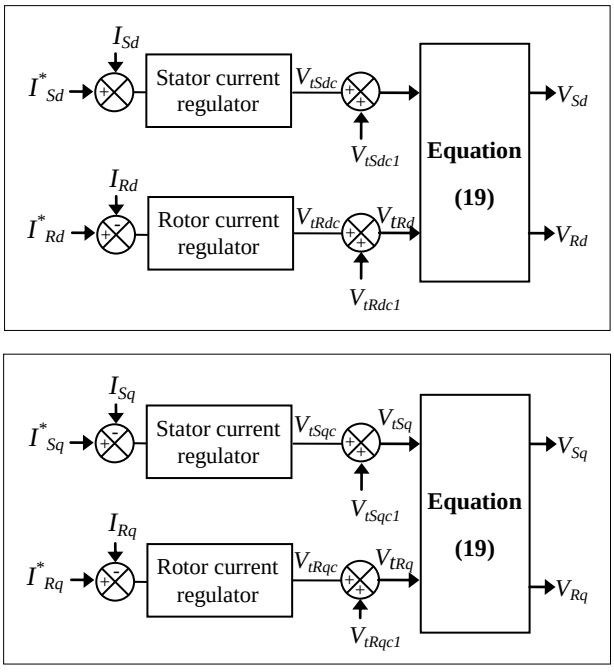

Fig. 3. Decoupling and regulation of the currents.

The current references are given by :

$$\begin{cases} I_{Sd}^{\ *} = \dfrac{1}{M_{SR}}\varphi_{Rd}^{\ *}, \quad I_{Sq}^{\ *} = \dfrac{L_R}{p.M_{SR}.\varphi_{Rd}^{\ *}}\ C_{em}^{\ *} \\ I_{Rd}^{\ *} = 0 \qquad\quad , \quad I_{Rq}^{\ *} = -\dfrac{1}{p.\varphi_{Rd}^{\ *}}\ C_{em}^{\ *} \end{cases} \quad (23)$$

Thus, figure 3 shows the control structure of the currents.

C. The speed regulation

Basing on relation (16) and the assumption to work with I_{Rd} equal to zero, the electromagnetic torque can be written as :

$$C_{em} = -p\ \varphi_{Rd} I_{Rq} = K_{em} I_{Rq} \quad (24)$$

Substituting (24) in (13), it results :

$$J\frac{d\Omega}{dt} = K_{em} I_{Rq} - f\,\Omega - C_r \quad (25)$$

Where K_{em} is the torque constant.

Thus, the speed transfer function can be expressed by:

$$\Omega(s) = \frac{K_{em}}{f + Js} I_{Rq}(s) - \frac{1}{f + Js} C_r(s) \quad (26)$$

$C_r(s)$ is a disturbing input, while $I_{Sq}(s)$ is main input.

Consequently, the block diagram of the speed regulation is given by figure 4.

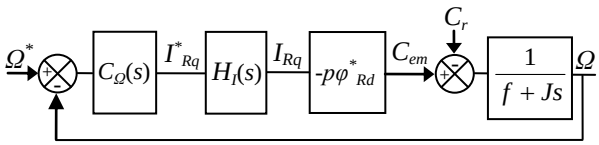

Fig. 4. Block diagram of the speed control.

5. Speed controllers synthesis

In this section, we have chosen to compare the performances of the DFIM with four different controllers : Proportional integral (PI), conventional sliding mode (SMC), second order sliding mode (SOSMC) and fuzzy second order sliding mode (FSOSMC).

A. Sliding mode controller (SMC)

The sliding mode technique is developed from variable structure control to solve the disadvantages of other designs of nonlinear control systems. The sliding mode is a technique to adjust feedback by previously defining a surface. The system which is

controlled will be forced to that surface, then the behavior of the system slides to the desired equilibrium point [17].

The main feature of this control is that we only need to drive the error to a *switching surface*. When the system is in *sliding mode*, the system behavior is not affected by any modeling uncertainties and/or disturbances. The design of the control system will be demonstrated for a nonlinear system presented in the canonical form [18] :

$$\dot{x} = f(x,t)+B(x,t)V(x,t),\ x\in R^n,\ V\in R^m, ran(B(x,t)) = m \quad (27)$$

with control in the sliding mode, the goal is to keep the system motion on the manifold *S*, which is defined as :

$$S = \{x : e(x, t)=0\} \quad (28)$$

$$e = x^* - x \quad (29)$$

Here *e* is the tracking error vector, x^* is the desired state, *x* is the state vector. The control input *u* has to guarantee that the motion of the system described in (27) is restricted to belong to the manifold *S* in the state space. The sliding mode control should be chosen such that the candidate Lyapunov function satisfies the Lyapunov stability criteria :

$$\vartheta = \frac{1}{2}S(x)^2, \quad (30)$$

$$\dot{\vartheta} = S(x)\dot{S}(x). \quad (31)$$

This can be assured for :

$$\dot{\vartheta} = -\eta|S(x)| \quad (32)$$

Here η is strictly positive.

Essentially, equation (30) states that the squared "distance" to the surface, measured by $e(x)^2$, decreases along all system trajectories. Therefore (31), (32) satisfy the Lyapunov condition. With selected Lyapunov function the stability of the whole control system is guaranteed. The control function will satisfy reaching conditions in the following form:

$$U^{com} = U^{eq} + U^n \quad (33)$$

Here U^{com} is the control vector, U^{eq} is the equivalent control vector, U^n is the correction factor and must be calculated so that the stability conditions for the selected control are satisfied.

$$U^n = K\ \text{sat}((S(x)/\delta) \quad (34)$$

sat($(S(x)/\delta)$ is the proposed saturation function, δ is the boundary layer thickness. In this paper we propose the Slotine method [19]:

$$S(X)=\left(\frac{d}{dt}+\lambda\right)^{n-1} e \quad (35)$$

Here, *e* is the tracking error vector, λ is a positive coefficient and *n* is the relative degree.

In our study, we choose the error between the measured and reference speed of the DFIM as sliding mode surface, so we can write the following expression :

$$S = \Omega^* - \Omega \quad (36)$$

The first order derivate of (29), gives :

$$\dot{S} = \dot{\Omega}^* - \dot{\Omega} \quad (37)$$

Substituting the expression of $\dot{\Omega}$ equation (26) in equation (30), we obtain:

$$\dot{S} = \dot{\Omega}^* - \frac{K_{em}}{J} I_{Rq} - \frac{f}{J}\ \Omega - \frac{C_r}{J} \quad (38)$$

I_{qr} will be the component of the control vector used to constraint the system to converge to *S*=0. The control vector U_{eq} is obtain by imposing $\dot{S} = 0$ so the equivalent control components are given by the following relation :

$$U_{eq} = -\frac{f}{K_{em}}\cdot\Omega + \frac{J}{K_{em}}\dot{\Omega}^* - \frac{C_r}{K_{em}} \quad (39)$$

To obtain good performances, dynamic and commutation around the surface, the control vector is imposed as follows [18]:

$$U = U_{eq} + K\cdot\text{sign}(S) \quad (40)$$

The sliding mode will exist only if the following condition is met :

$$S\cdot\dot{S} < 0 \quad (41)$$

B. Second order sliding mode controller (SOSMC)

Sliding mode control (SMC) is one of the most interesting nonlinear control approaches. Nevertheless, a few drawbacks arise in its practical implementation, such as chattering phenomenon and undesirable mechanical effort [20]. In order to reduce the effects of these problems, second order sliding mode seems to be a very attractive solution [21].

This method generalizes the essential sliding mode idea by acting on the higher order time derivatives of the sliding manifold, instead of

influencing the first time derivative as it is the case in SMC, therefore reducing chattering and avoiding strong mechanical efforts while preserving SMC advantages [22].

In order to ensure the DFIM's speed convergence to their reference, a second order sliding mode control (SOSMC) is used. Considering the sliding mode surface given by (29), the following expression can be written:

$$\begin{cases} \dot{S} = \dot{\Omega}^{*} - \dfrac{K_{em}}{J} I_{Rq} - \dfrac{f}{J}\ \Omega - \dfrac{C_r}{J} \\ \ddot{S} = Y(t,x) + \Lambda(t,x) I_{Rq} \end{cases} \quad (42)$$

Where $Y(t,x)$ and $\Lambda(t,x)$ are uncertain functions which satisfy:

$$Y > 0,\ |Y| > \lambda,\ 0 < K_m < \Lambda < K_M$$

Basing on the super twisting algorithm introduced by Levant in [23], the proposed high order sliding mode controller contains two parts [24]:

$$I_{Rq} = v_1 + v_2 \quad (43)$$

With

$$\dot{v}_1 = -k \cdot sign(S)$$

$$v_2 = -l \cdot |S|^{\gamma} \cdot sign(S)$$

In order to ensure the convergence of the sliding manifolds to zero in finite time, the gains can be chosen as follows [24].

$$\begin{cases} k > \dfrac{\lambda}{K_m} \\ l^2 \geq \dfrac{4\lambda}{K_m^2} \dfrac{K_M (k+\lambda)}{K_m (k-\lambda)} \\ 0 < \gamma \leq 0.5 \end{cases}$$

C. Fuzzy second order sliding mode controller (FSOSMC)

As mentioned in the previous section, the main disadvantage of the SMC is the chattering phenomenon. Among all the solutions used nowadays to decrease the effect of this phenomenon on the DFIM control, the second order sliding mode technique seems very interesting. Indeed, this method has proven in several studies and research applications its effectiveness in minimizing this undesirable phenomenon which is mainly due to the presence of a discontinuous control term containing the *sign* function.

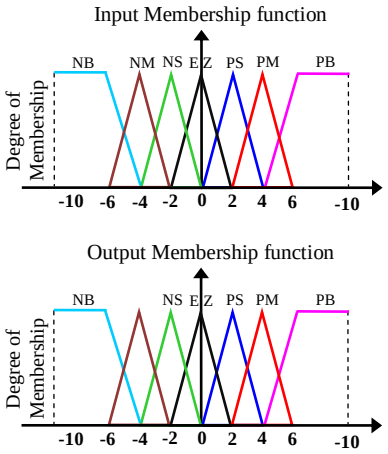

Fig. 5. Fuzzy sets and its memberships functions.

In order to improve the SOSMC of the DFIM and more and more decrease the adverse effect caused by the *sign* function, we propose in this paper to use the fuzzy second order sliding mode control (FSOSMC).

For the proposed FSOSMC, the universes of discourses are first partitioned into the seven linguistic variables NB, NM, NS, EZ, PS, PM, PB, triangular and trapezoidal membership functions are chosen to represent the linguistic variables for the inputs and outputs of the controllers.

The fuzzy labels used in this study are negative big (NB), negative medium (NM), negative small (NS), equal zero (EZ), positive small (PS), positive medium (PM) and positive big (PB).

These choices are described in figure 5.

6. Simulation results and discussions

In this section, simulations are realized with a 1.5 KW motor coupled to a 220V/50Hz grid. The bloc diagram of the proposed control scheme of the DFIM is given by figure 6. Parameters of the machine are given in appendix. In the aim to evaluate the performances of the four controllers: PI, SMC, SOSMC and FSOSMC, three categories of tests have been realized: pursuit test, sensitivity to the load torque variation and robustness against machine parameter variations.

A. Pursuit test

The objective of this test is the study of the four controllers' behavior in reference tracking, while the load torque is considered equal to zero. The simulation results are presented in figures 7 and 8. As it's shown by figure 7, for the four controllers, the

mechanical speed tracks almost perfectly their reference but with an important response time for the PI controller compared to the other controllers. Therefore it can be considered that the three types of sliding mode controllers have a very good performance for this test. On the other hand, figure 8 shows the harmonic spectrum of the electromagnetic torque of the DFIM obtained using Fast Fourier Transform (FFT) technique for the three controllers. It can be observed that the total harmonic distortion (THD) is clearly reduced for FSOSMC (THD = 22.86%) when compared to SOSMC (THD = 45.78%), SMC (THD = 49.62%) and PI (THD = 45.13%). Therefore it can be concluded that the

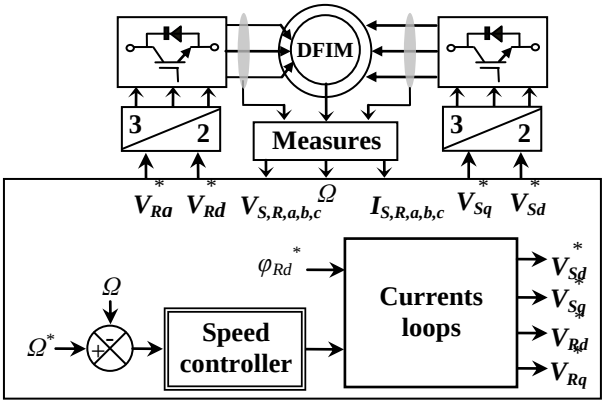

Fig. 6. Block diagram of the proposed control scheme of the DFIM.

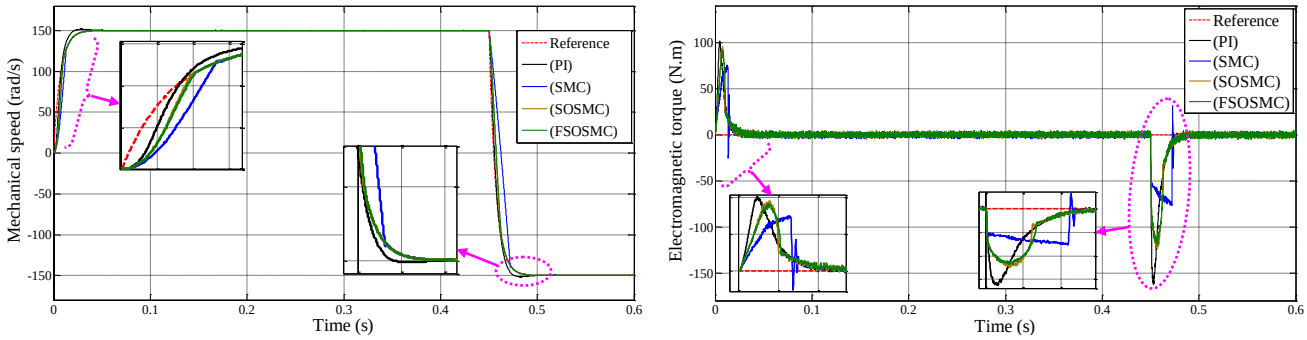

Fig. 7. Reference tracking test.

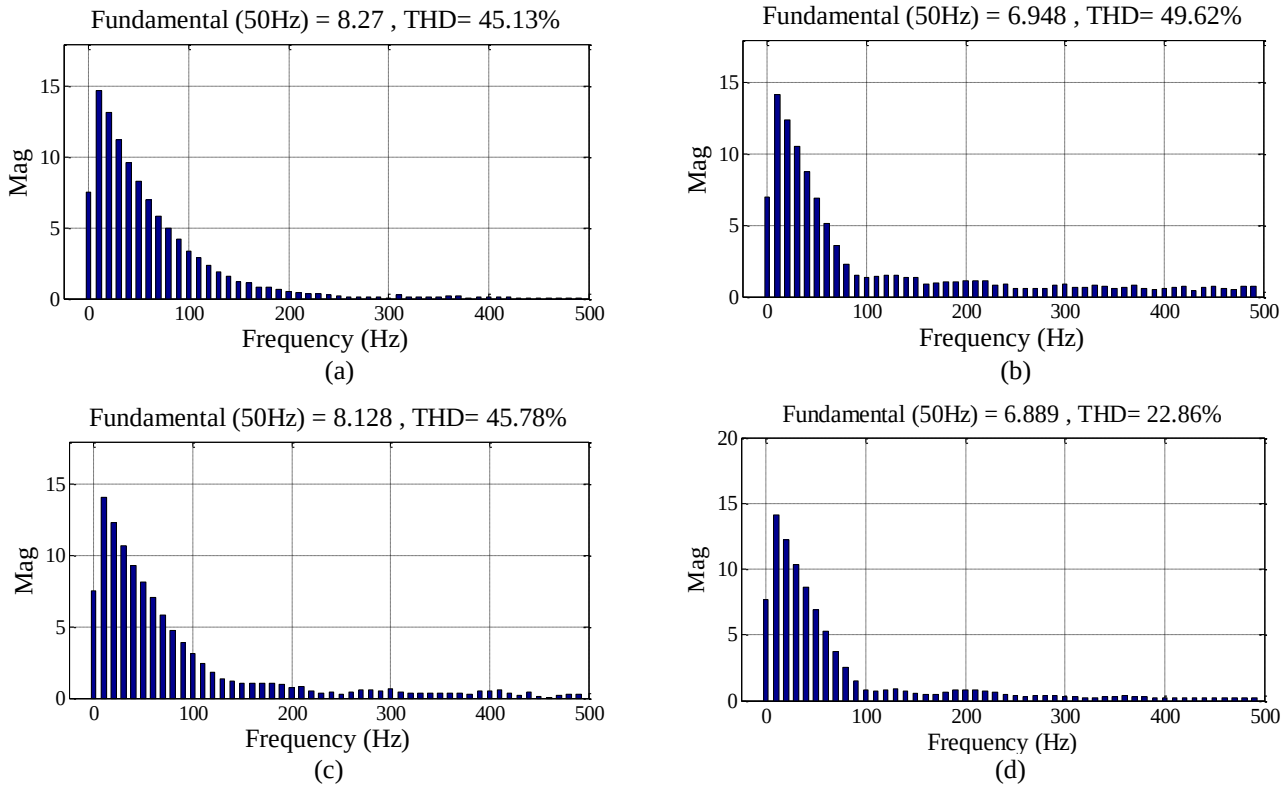

Fig. 8. Spectrum harmonic of the electromagnetic torque for (a) PI, (b) SMC, (c) SOSMC, (d) FSOSMC.

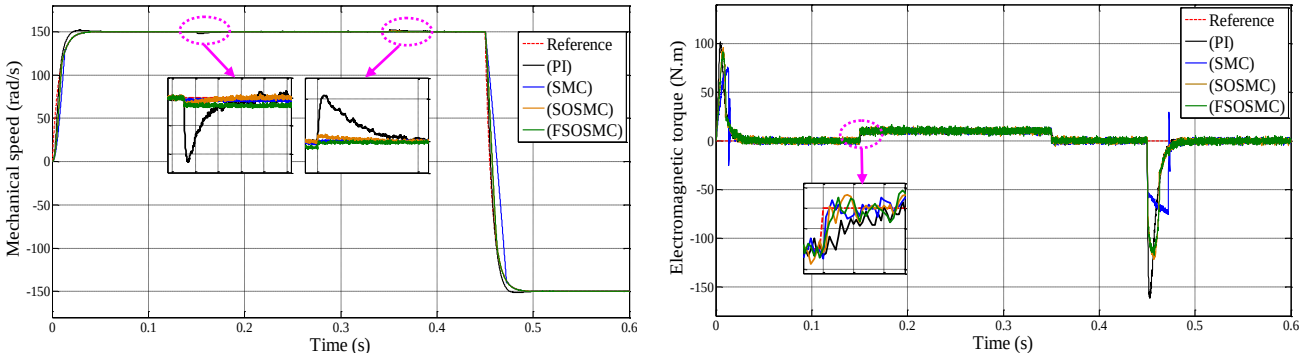

Fig. 9. Sensitivity to the load torque variation.

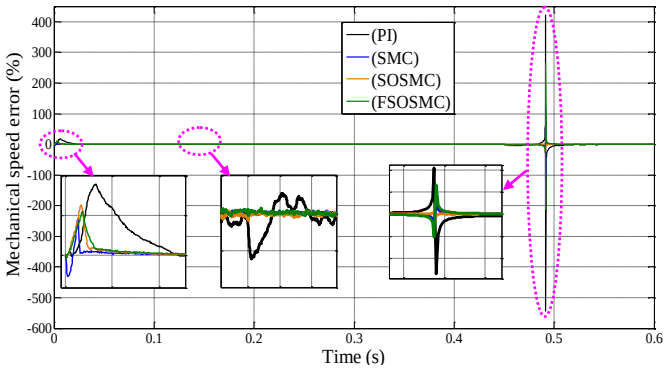

Fig. 10. Robustness test (J=2*J_n).

proposed controller (FSOSMC) is the most effective in eliminating chattering phenomenon. However, we note that despite the use of FLSOSMC, THD torque remains fairly high. This is principally due to the use of two power converters, which represents one of the major disadvantages of such configuration of DFIM.

B. Sensitivity to the load torque variation

The aim of this test is to analyze the influence of the load torque variation on the DFIM response for the four controllers. For this objective and in the in the time interval t = 0.15s and t = 0.35s, the load torque is kept equal to its nominal value C_{rn} =10 N.m. The simulation results are shown in figure 9. This figure express that the effect produced by the load torque variation is very clear on the speed curve of the system with PI controller, while the effects are almost negligible for the system with the three other controllers. It can be noticed that these last have a nearly perfect speed disturbance rejection, indeed; only very small speed variations can be observed (fewer than 2%). This result is very attractive for speed control applications to ensure stability when the load torque is varying.

C. Robustness

In order to test the robustness of the used controllers, the machine inertia has been doubled. The results presented in figure 10 show that inertia variation presents a clear effect on the speed responses (in the error curves) of all used controllers and that the effect appears more significant for PI controller than that with the three other ones. Thus it can be concluded that these last are robust against this parameter variation.

7. Conclusion

A new robust control method based on variable structure technique and fuzzy logic of a DFIM supplied by two matrix converters has been presented in this paper. In the first step, we started with a study of modeling on the matrix converter controlled by the Venturini modulation technique. In second step, we adopted a vector control strategy in order to make the behavior of the DFIM like a DC motor, i.e. a decoupling between the magnetic flux and the electromagnetic torque. Four types of controllers are synthesized and compared in the third step in the goal to control the speed of the DFIM. The various results obtained in simulation show the FSOSMC

robustness to the system and load parameters disturbances. In addition the speed follow without overshooting, decoupling, stability and equilibrium convergence are ensured on the entire variation interval. The results obtained with this FSOSMC are very interesting compared to the other types of the sliding mode controllers especially in eliminating of the chattering phenomenon. The static inverter and the control nature with variable structure introduce high frequency undulations which appear on the torque level. However, with the use of second order sliding mode and a high modulation index, we can reduce the couple fluctuations considerably. Moreover this control has the advantage of being easily implemented by a program control.

Appendix

Table 1. Nomenclature.

Symbol	Significance
S, R	Rotor and stator indices,
d, q	Direct and quadrate indices for orthogonal components,
$\bar{x}$	Variable complex such as: $\bar{x} = \mathrm{Re}[\bar{x}] + j\ \mathrm{Im}[\bar{x}]$ with $j^2 = -1$. $\bar{X}$ it can be a voltage as $\bar{V}$, a current as $\bar{I}$ or a field as $\bar{\varphi}$,
R_S, R_R	Stator and rotor resistances,
L_S, L_R	Stator and rotor inductances,
M_{SR}	Mutual inductance,
p	Number of pairs poles,
θ	Absolute rotor position,
θ_S, θ_R	Stator and rotor flux absolute positions,
σ	Leakage flux total coefficient ($\sigma = 1 - M_{SR}^2 / L_S L_R$),
ω_S	Stator current frequency (rad/s),
J	Inertia (J_n nominal value of J),
f	Coefficient of viscous frictions,
C_r	Load torque,
C_{em}	Electromagnetic torque.

Table 2. The DFIM parameters.

Parameters	Value	IS-Unit
Stator voltage	220	V
Rotor voltage	130	V
Stator/rotor frequency	50	Hz
Stator resistance	1.75	Ω
Rotor resistance	1.68	Ω
Stator inductance	0.295	H
Rotor inductance	0.104	H
Mutual inductance	0.165	H
Inertia	0.01	$Kg.m^2$

References

1. Anaya-Lara, O., Jenkins, N., Ekanayake, J., Cartwright, P., Hughes, M.: *Wind energy generation*. In: Wiley, 2009.
2. Djeriri, Y., Meroufel, A., Massoum, A. and Z. Boudjema.: *A comparative study between field oriented control strategy and direct power control strategy for DFIG*. In: Journal of Electrical Engineering, Vol. 14, No. 2, pp. 159-167, 2014.
3. Pöller, M. A.: *Doubly-fed induction machine models for stability assessment of wind farms*. In: Proc. IEEE PowerTech, Bologna, Italy, Vol. 3, 23-26 June 2003.
4. Brekken, T., Mohan, N.: *A novel doubly-fed induction wind generator control scheme for reactive power control and torque pulsation compensation under unbalanced grid voltage conditions*. In: IEEE 34th Annual Power Electronics Specialist Conference, 2003, PESC'03, Vol. 2, pp. 760-764, 15-19 June 2003.
5. Leonhard, W.: *Control of electrical drives*. In: 2nd ed. New York: Springer-Verlag, 1996.
6. Kawabata, Y., Ejiogu, E. and Kawabata, T.: *Vector controlled double inverter fed wound rotor induction motor suitable for high power drives*. In: IEEE Trans. Ind. Appl., Vol. 35, No. 5, pp. 1058-1066, Sep./Oct. 1999.
7. Bonnet, F., Vidal, P. E. and Pietrzak-David, M.: *Dual direct torque control of doubly fed induction machine*. In: IEEE Trans On Industrial Electronics, Vol. 54, No. 5, October 2007.
8. Lee, M. Y., Wheeler, P. and Klumpner, C.: *Space-vector modulated multilevel matrix converter*. In: IEEE Trans. On Industrial Electronics, vol. 57, No. 10, pp. 3385-3394, October 2010.
9. Martinez, M. I., Tapia, G., Susperregui, A., and Camblong, H.: *Sliding-mode control for DFIG rotor and grid-side converters under unbalanced and harmonically distorted grid voltage.* In: IEEE Trans. On Energy Conversion, Vol. 27, No. 2, pp. 328-339, March 2000.
10. Hu, J., Nian, H., Hu, B., He, Y. and Zhu, Z. Q.: *Direct active and reactive power regulation of DFIG using sliding-mode control approach*. In: IEEE Trans. On Energy Conversion, Vol. 25, No. 4, pp. 1028–1039, Dec. 2010.
11. Lopez, J., Sanchis, P., Roboam, X., Marroyo, L.: *Dynamic behavior of the doubly fed induction generator during three-phase voltage dips*. In: IEEE Transaction on Energy Conversion, pp. 709-717, 22 (September (3)) 2007.
12. Cupertino, F., Naso, D., Mininno, E., Turchiano, B. : *Sliding-mode control with double boundary layer for robust compensation of payload mass and friction in linear motors*. In: IEEE Trans. On Industry Applications, Vol. 45, No. 5, pp. 1688-1696, Sep./Oct 2009.

13. Chikha, S., Barra, K., Reama, A.: *Predictive current control of a wind energy conversion system based DFIG via direct matrix converter*. In Proc. of IEEE IREC 2015, pp. 1-7, 24-26 March 2015.
14. Z. Boudjema, A. Meroufel, E. Bounadja and Y. Djerriri.: *Nonlinear control of a doubly fed induction generator supplied by a matrix converter for wind energy conversion systems*. In: Journal of Electrical Engineering, Vol. 13, No. 4, pp. 269–276, 2013.
15. Venturini M., *A new sine wave in sine wave out conversion technique which eliminates reactive elements*, In: Proc Power con 7, San Diego, CA, pp E3-1, E3-15, 27-24 March 1980.
16. Okedu, K. E., Uhunmwangho, R.: *Matrix converter control for DFIG*. In Proc. of IEEE International Conference on Emerging & Sustainable Technologies for Power & ICT in a Developing Society (NIGERCON), pp. 273-277, 14-16 November 2013.
17. Wai, R. J., and Chang, J. M.: *Implementation of robust wavelet-neural-network sliding-mode control for induction servo motor drive.* In: IEEE Trans. On Industrial Electronics, Vol. 50, No. 6, pp. 1317-1334, December 2003.
18. Sun, T., Chen, Z., Blaabjerg, F.: *Flicker study on variable speed wind turbines with doubly fed induction generators*. In: IEEE Transactions on Energy Conversion, pp. 896–905, 20 (December (4)) 2005.
19. J. J. E. Slotine and W. Li, Applied Nonlinear Control. Englewood Cliffs, NJ: Prentice–Hall, 1991.
20. Wang, W. J, and Chen, J. Y.: *Passivity-based sliding mode position control for induction motor drives*. In: IEEE Trans. On Energy Conversion, Vol. 20, No. 2, pp. 316-321, June 2005.
21. Rashed, M., Goh, K. B., Dunnigan, M. W. MacConnell, P. F. A., Stronach, A. F. and Williams, B. W.: *Sensorless second-order sliding-mode speed control of a voltage-fed induction-motor drive using nonlinear state feedback.* In: IEE Proc.-Electr. Power Appl., Vol. 152, No. 5, pp. 1127-1136, September 2005.
22. Morsy, M. A. A., Said, M., Moteleb, A., Dorrah, H., T.: *Design and implementation of fuzzy sliding mode controller for switched reluctance motor*. I: Proceedings of the International MultiConference of Engineers and Computer Scientists, Vol. 2, IMECS, Hong Kong, 19-21 March 2008.
23. Levant, A., Alelishvili, L.: *Integral high-order sliding modes*. In : IEEE Trans. Autom. Control, Vol. 52, No. 7, pp. 1278-1282, July 2007.
24. Benelghali, S., Benbouzid, M. E. H., Charpentier, J. F., Ahmed-Ali, T. and Munteanu, I.: *Experimental validation of a marine current turbine simulator: Application to a PMSG-based system second-order sliding mode control*. In: IEEE Trans. Ind. Electron., Vol. 58, No. 1, pp. 118-126, January 2011.